Paramagnetic ^{13}C and ^{15}N NMR Analyses of Cyanide- ($^{13}C^{15}N$-) Ligated Ferric Peroxidases: The Push Effect, Not Pull Effect, Modulates the Compound I Formation Rate[†]

Daisuke Nonaka,[‡,§] Hiroyuki Wariishi,[‡] and Hiroshi Fujii*[,§]

Faculty of Agriculture, Kyushu University, Hakozaki, Fukuoka 812-8581, Japan, and Institute for Molecular Science and Okazaki Institute for Integrative Bioscience, National Institutes of Natural Sciences, Myodaiji, Okazaki 444-8787, Japan

Received October 31, 2008; Revised Manuscript Received December 16, 2008

ABSTRACT: Paramagnetic ^{13}C and ^{15}N NMR spectroscopy of heme-bound cyanide ($^{13}C^{15}N$) was utilized to quantitatively distinguish the electron donor effect (the push effect) from the proximal histidine and hydrogen-bonding effect (the pull effect) from the distal amino acid residues in cytochrome *c* peroxidase (CcP), ascorbate peroxidase (APX), lignin peroxidase (LiP), and manganese peroxidase (MnP). Paramagnetic ^{13}C NMR signals of heme-bound $^{13}C^{15}N$ of these peroxidases were observed in a wide range, −3501 ppm (CcP), −3563 ppm (APX), −3823 ppm (MnP), and −3826 ppm (LiP), while paramagnetic ^{15}N NMR signals of those were detected in a narrow range, 574 ppm (ARP), 605 ppm (CcP), 626 ppm (LiP), and 654 ppm (MnP). Detailed analysis, combined with the previous results for horseradish peroxidase and *Arthromyces ramosus* peroxidase, indicated that the push effect is quite different among these peroxidases while the pull effect is similar. More importantly, a strong correlation between the ^{13}C NMR shift (the push effect) and the compound I formation rate was observed, indicating that the push effect causes a variation in the compound I formation rate. Comparison of the ^{13}C and ^{15}N NMR results of these peroxidases with their crystal structures suggests that the orientation of the proximal imidazole plane to the heme N−Fe−N axis controls the push effect and the compound I formation rate of peroxidase.

Peroxidases are a ubiquitous class of enzymes that catalyze the oxidation of a wide variety of organic and inorganic substrate molecules with hydrogen peroxide. Most peroxidases contain an iron protoporphyrin IX as their prosthetic group and share common reaction intermediates, compound I and compound II, as described below (*1*). The initial step in the catalytic mechanism is heterolysis of the O−O bond of hydrogen peroxide, resulting in the two-electron-deficient compound I (Fe^{4+}=O, R•) and water, where R is the organic moiety of the heme or an amino acid residue. Then, compound I is reduced back to the resting state by sequential one-electron oxidation of two substrates, SH, via the intermediate compound II (Fe^{4+}=O).

$$\text{resting state}\,(Fe^{3+}) + H_2O_2 \rightarrow \text{compound I}\,(Fe^{4+}{=}O,\ R\bullet) + H_2O$$

$$\text{compound I}\,(Fe^{4+}{=}O,\ R\bullet) + SH \rightarrow \text{compound II}\,(Fe^{4+}{=}O) + S\bullet$$

$$\text{compound II}\,(Fe^{4+}{=}O) + SH \rightarrow \text{resting state}\,(Fe^{3+}) + S\bullet + H_2O$$

The ability to react rapidly with hydrogen peroxide to form compound I discriminates peroxidases from other classes of heme proteins. This characteristic reactivity must result entirely from the influence of the protein around heme, since most heme proteins possess the same iron protoporphyrin IX prosthetic group. Detailed crystallographic studies on cytochrome *c* peroxidase (CcP),[1] ascorbate peroxidase (APX), *Arthromyces ramosus* peroxidase (ARP), lignin peroxidase (LiP), manganese peroxidase (MnP), and horseradish peroxidase (HRP) have firmly established the similarity of the active site structures in peroxidases (*2*−*7*): His and Arg in the distal side and the heme-bound His and Asp in the proximal side (Figure 1). The distal His is thought to function as a general acid/base catalyst that assists in deprotonating hydrogen peroxide to facilitate its binding to the heme iron and protonation of heme-bound hydroperoxide to promote compound I formation via its heterolytic O−O bond cleavage (*8*). Arg is proposed as a stabilizer of the

[†] This work was supported by grants from CREST, Japan Science and Technology Agency, and the Global COE Program, the Japan Science Promotion Society (H.F.) and by Research Fellowships of the Japan Society for the Promotion of Science for Young Scientists (D.N.).

* To whom correspondence should be addressed. Tel: +81-564-59-5578. Fax: +81-564-59-5600. E-mail: hiro@ims.ac.jp.

[‡] Kyushu University.

[§] National Institutes of Natural Sciences.

[1] Abbreviations: HRP, horseradish peroxidase; ARP, *Arthromyces ramosus* peroxidase; CIP, *Coprinus cinereus* peroxidase; APX, ascorbate peroxidase; CcP, cytochrome *c* peroxidase; MnP, manganese peroxidase; LiP, lignin peroxidase; SW-Mb, sperm whale myoglobin; Hb, human hemoglobin; HH-cyt *c*, horse heart cytochrome *c*; rat-HO, rat heme oxygenase; FixL, *Sinorhizobium meliloti* FixL; TMS, tetramethylsilane.

10.1021/bi802030a CCC: $40.75
Published on Web 01/20/2009

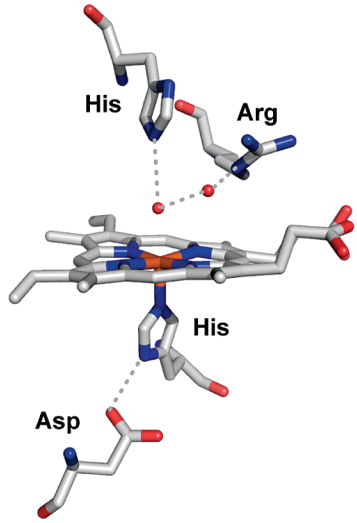

FIGURE 1: Conserved structural characteristics of the heme active site in CCP. Possible hydrogen bonds (within 3 Å) are shown by dotted lines. The image was created from the crystal structural data (PDB code 2CYP) (*2*) using the Pymol Molecular Graphic System (*63*).

transition state for compound I formation (*9*). Asp interacts with the proximal imidazole ligand in the heme-bound His, which should increase the electron density of the heme iron, facilitating compound I formation and stabilizing the ferryl (Fe^{4+}) oxidation states of compound I and compound II. The hydrogen-bonding interactions of His and Arg to heme iron-bound hydroperoxide, termed the pull effect, and the increased electron donation of the proximal imidazole ligand by Asp, called the push effect, lead to the rapid reaction of peroxidases with hydrogen peroxide (*10*−*15*).

While peroxidases have common structural characteristics to react with hydrogen peroxide as mentioned above, rates of compound I formation among peroxidases are significantly different. CcP and APX, which belong to class I peroxidase, form compound I with 10^7−10^8 M^{-1} s^{-1} whereas LiP, MnP, and ARP, which are classified as a class II peroxidase, show ∼100-fold slower formation rates, 10^5−10^6 M^{-1} s^{-1}, and HRP, a class III peroxidase, has ∼10-fold slower rate (*16*−*38*). These results suggest the strength of the push and pull effects is modulated in each class of peroxidases. However, direct comparison of the push and pull effects among peroxidases has not been reported because of the absence of spectroscopy that is sensitive to both push and pull effects. The molecular mechanism to control the compound I formation rate would be essential to understand peroxidase function at a molecular level.

To address this question, in this study, we carried out paramagnetic ^{13}C and ^{15}N NMR spectroscopy of heme-bound cyanide ($^{13}C^{15}N$) of ferric CcP, APX, LiP, and MnP. Recently, we showed that the ^{13}C NMR signal of the heme-bound $^{13}C^{15}N$, which showed an extremely large upfield shift at around −3500 to −4000 ppm from tetramethylsilane (TMS), was a good indicator for the push effect of the proximal ligand; the ^{13}C NMR paramagnetic shift increases with a decrease in the push effect, while the ratio of the ^{15}N NMR shift over the ^{13}C NMR shift indicated the pull effect; the ratio decreased with an increase in the pull effect (*39*−*41*). In combination with previous results for ferric HRP and ARP (*40*), this study clearly indicated that the push effect in each class of peroxidases differs significantly while the pull effect is similar in all classes. Furthermore, a strong correlation between the push effect and the compound I formation rate was found, indicating that the push effect causes a variation in the compound I formation rate. Comparison of the ^{13}C and ^{15}N NMR results of these peroxidases with their crystal structures suggests that the orientation of the proximal imidazole plane to the heme N−Fe−N axis modulates the push effect and the compound I formation rate of peroxidase.

MATERIALS AND METHODS

Chemicals. Isotope-labeled potassium cyanide ($K^{13}C^{15}N$) was purchased from New England Biolabs. All other chemicals were of reagent grade. Solutions were prepared using Milli-Q water (Millipore) or D_2O (Wako Pure Chemicals).

Enzyme Preparation. MnP isozyme 1 (H3) and LiP isozyme 2 (H8) were prepared from the extracellular medium of acetate-buffered, agitated cultures of *Phanerochaete chrysosporium*, as previously described (*31, 42*−*44*), except that 0.175 g/L $MnSO_4$ was added to the medium for maximal induction of MnP expression (*45*). Initially, as Banci et al. reported (*46*), purified MnP showed a broadened ^1H NMR spectrum, indicating that enzyme-bound manganese ions were present in our sample. Hence, to eliminate the Mn^{2+} paramagnetic effect, the MnP sample was treated with 1 mM ethylenediaminetetraacetic acid, pH 7.2, for 1 h and was then passed through Sephadex G-100 (1.6 cm × 90 cm; Amersham Bioscienecs) equilibrated with 50 mM phosphate, pH 7.2. The purified enzymes were electrophoretically homogeneous. RZ (A_{408}/A_{280}) values were 5.1 for MnP and 4.6 for LiP.

ARP was purchased from Nakarai Tesque, Inc., and was purified using DEAE-Sepharose Fast Flow (Amersham Biosciences). The enzyme was dialyzed against 1 mM $CaCl_2$ for 16 h. The purified enzyme showed an RZ value of approximately 3.

CcP from *Saccharomyces cerevisiae* was heterologously expressed in *Escherichia coli* and purified as described previously (*47*). Chromatographic purification and subsequent crystallization by dialysis against deionized water gave the crystallized enzyme, which had a PZ value (A_{408}/A_{280}) of 1.2.

His-tagged pea cytosolic APX was also expressed in *E. coli* and purified using Ni-NTA resin (Qiagen) and Sephacryl S-200 (GE Healthcare) as previously described (*48*) with some modifications. The purified enzyme exhibited a Soret peak at 403 nm and an RZ value (A_{408}/A_{280}) of 2.0.

Determination of the Compound I Formation Rate of ARP. Transient-state kinetic measurements were conducted using a Photal RA 401S rapid reaction analyzer (Otsuka Electronics Co. Ltd.) equipped with a 1 cm observation cell at 25.0 ± 0.1 °C. The formation rate of ARP compound I was determined at 400 nm. One reservoir contained ferric ARP (ca. 2 μM) in water, and the other reservoir contained H_2O_2 (10−40 μM) in 40 mM phosphate, pH 7.0. The pseudo-first-order rate constants were obtained by a nonlinear least-squares computer analysis of exponential traces.

Paramagnetic NMR Analysis. ^1H, ^{13}C, and ^{15}N NMR spectra of peroxidases were obtained on a JEOL Lambda-500 spectrometer. The enzyme samples (in >60% D_2O) were prepared using either 100 mM sodium acetate buffer, pH

6.0, containing 0.1 mM $CaCl_2$ (for LiP and MnP), or 100 mM potassium phosphate, pH 7.0 (for CcP and APX), and then were filtered through a 0.2 μm pore cellulose−acetate filter. The concentration of the enzyme sample was adjusted to 2−4 mM using Amicon Ultra-15 (Millipore). Enzyme samples were stable, and no spectral changes were observed after 1 week of storage, although the enzyme concentration was high. After concentration of the enzyme solution, isotope-labeled cyanide was added to a final concentration of 10 mM to form the cyanide-ligated enzyme sample. ^{13}C NMR spectra were obtained at sweep widths of 200 kHz at 125.27 MHz using 4K data points. ^{15}N NMR spectra were obtained at sweep widths of 100 kHz at 50.73 MHz using 4K data points. The pulse repetition time and pulse width were 0.075 s and 8 μs, respectively. Typically, 500000 transients were collected for both ^{13}C and ^{15}N NMR measurements. The chemical shift values of the ^{13}C and ^{15}N NMR spectra were referenced to external TMS in chloroform and to sodium nitrate ($^{15}NO_3^-$) in deuterium oxide, respectively. The ^{13}C and ^{15}N NMR data were analyzed by the following method (*39*−*41*). The observed NMR paramagnetic shifts of heme-bound $^{13}C^{15}N$ are the sum of the diamagnetic shift that is the NMR shift of the original cyanide ion and the isotropic paramagnetic shift that is the NMR shift induced by the paramagnetic ferric heme iron center, as shown in eq 1.

$$\left(\frac{\Delta H}{H}\right)^{\text{par}} = \left(\frac{\Delta H}{H}\right)^{\text{iso}} + \left(\frac{\Delta H}{H}\right)^{\text{dia}} \quad (1)$$

The diamagnetic shifts of ^{13}C and ^{15}N NMR signals of heme-bound $^{13}C^{15}N$ could be estimated from the ^{13}C and ^{15}N NMR shifts of a diamagnetic compound such as potassium ferrocyanide, $K_4Fe(CN)_6$: ^{13}C, +177 ppm from TMS; ^{15}N, −111 ppm from $^{15}NO_3^-$ (*49, 50*). The isotropic paramagnetic shift consists of a dipolar shift arising from a through-space dipolar interaction between the ^{13}C or ^{15}N atom of cyanide and the ferric heme iron center and a contact shift resulting from the delocalization of electron spin into an orbital on the ^{13}C or ^{15}N atom, as shown eq 2.

$$\left(\frac{\Delta H}{H}\right)^{\text{iso}} = \left(\frac{\Delta H}{H}\right)^{\text{con}} + \left(\frac{\Delta H}{H}\right)^{\text{dip}} \quad (2)$$

The dipolar shifts were roughly estimated from EPR g parameters and the distance between the heme iron and the C or N atom of the iron bound cyanide, as shown in eq 3.

$$\left(\frac{\Delta H}{H}\right)^{\text{dip}} = \frac{\beta^2 S(S+1)}{9kT}\left(g_z^{\,2} - \frac{g_x^{\,2}+g_y^{\,2}}{2}\right)\left\langle\frac{3\cos^2\theta - 1}{r^3}\right\rangle \quad (3)$$

where β is the Bohr magneton, S is effective electron spin, g_x, g_y, and g_z are EPR g parameters, θ is the angle between the nucleus−metal vector and the z axis, r is the length of this vector, k is the Boltzman constant, and T is the temperature used in the NMR measurement. The ^{13}C and ^{15}N dipolar shifts for APX, CcP, and HRP were calculated to be +282 ppm and +74 ppm with the g and r values obtained from the EPR spectrum and X-ray crystal structure of the ferric cyanide complex of HRP (*51, 52*) while those for ARP, LiP, and MnP were calculated to be +305 ppm and +80 ppm with the g and r values for ferric cyanide complex of ARP, respectively (*40, 53*). The contact shifts were estimated from eq 2 with the dipolar shifts calculated above.

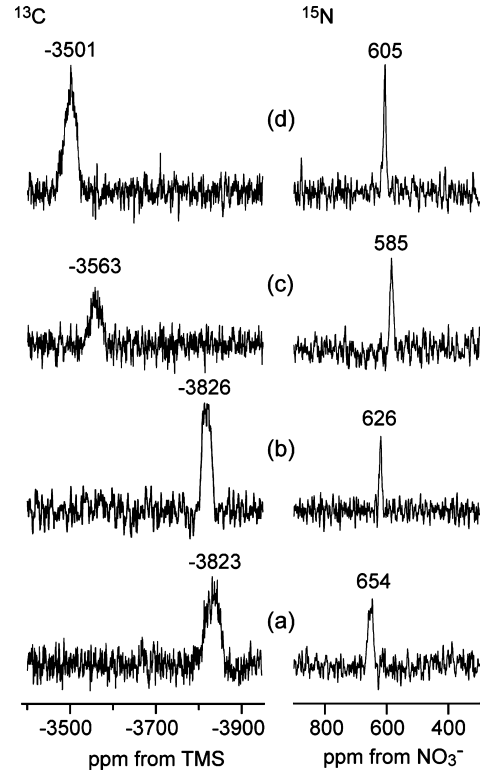

FIGURE 2: Paramagnetic ^{13}C NMR and ^{15}N NMR spectra of heme-bound $^{13}C^{15}N^-$ in ferric peroxidases. ^{13}C NMR (left panel) and ^{15}N NMR (right panel) spectra of (a) MnP, (b) LiP, (c) APX, and (d) CcP are shown. The sample concentrations used were ~4 mM in 100 mM acetate, pH 6.0, containing 1 mM $CaCl_2$ for LiP and MnP and in 100 mM potassium phosphate, pH 7.0, for the other enzymes.

RESULTS AND DISCUSSION

Paramagnetic ^{13}C and ^{15}N NMR Spectroscopy. ^1H NMR spectra of cyanide complexes of CcP, APX, LiP, and MnP were nearly identical to previously reported spectra (data not shown) (*29, 46, 54, 55*), indicating that the heme environments of these enzymes were intact, even at concentrations as high as 2−4 mM.

^{13}C NMR spectra of heme-bound $^{13}C^{15}N$ of ferric cyanide complexes of LiP, MnP, CcP, and APX are shown in Figure 2 (left panel). The ^{13}C NMR signals of heme-bound $^{13}C^{15}N$ for these peroxidases were observed in the far upfield region, as reported for other heme proteins. The paramagnetic shifts for class II peroxidases (−3826 ppm for LiP and −3823 ppm for MnP) were much greater than the shift obtained previously for the class III peroxidase (HRP: −3612 ppm) (Table 1) but relatively close to the shift for other class II peroxidases (ARP: −3699 ppm). In contrast, much smaller paramagnetic shifts were observed for the class I peroxidases (−3501 ppm for CcP and −3563 ppm for APX).

Paramagnetic ^{15}N NMR spectra of heme-bound $^{13}C^{15}N$ of ferric cyanide complexes of LiP, MnP, CcP, and APX are shown in Figure 2 (right panel). In contrast to the ^{13}C NMR signals, ^{15}N NMR signals were sharp and observed in the downfield region at around 600 ppm. The upfield shifts of the ^{13}C NMR signals and the downfield shifts of the ^{15}N NMR signals are reasonable to the spin polariza-

Table 1: ^{13}C and ^{15}N NMR Shifts and Compound I Formation Rates of Heme Peroxidases and Heme Proteins

	^{13}C NMR shift[a]		^{15}N NMR shift[b]					
	observed	contact	observed	contact	^{15}N /^{13}C	ref	compound I formation rate[c] (M^{-1} s^{-1})	ref
Class I (Intracellular)								
APX[d]	−3563	−4022	585	622	0.155	this study	$(7.3 \pm 1.0) \times 10^7$	*16*−*19*
CcP[d]	−3501	−3960	605	642	0.162	this study	$(4.0 \pm 0.7) \times 10^7$	*20*−*23*
Class II (Fungal Secretory)								
ARP	−3699	−4181	574	605	0.145	*40*	$(9.4 \pm 1.3) \times 10^{6\,f}$	*24*−*26*
LiP[e]	−3826	−4308	626	657	0.153	this study	$(5.1 \pm 0.1) \times 10^5$	*27*−*30*
MnP[e]	−3823	−4305	654	685	0.159	this study	$(3.0 \pm 1.6) \times 10^6$	*31*−*34*
Class III (Plant Secretory)								
HRP	−3612	−4071	576	613	0.151	*40*	$(1.7 \pm 0.1) \times 10^7$	*35*−*38*
Other Heme Proteins								
SW-Mb	−4145	−4724	951	942	0.199	*39*		
Hb (α-subunit)	−4074	−4622	975	980	0.212	*39*		
HH-cyt *c*	−3761	−4359	856	854	0.196	*39*		
rat-HO	−3750	−4257	818, 797	814	0.191	*40*		
FixL	−4128	−4733	905	895	0.189	*41*		

[a] ppm from TMS. [b] ppm from $^{15}NO_3^-$. [c] Average value of four previous reports. [d] EPR *g* values and geometric parameters used were those of HRP (*40*). [e] EPR *g* values and geometric parameters used were those of ARP (*40*). [f] One of four data is from this study.

tion mechanism from the low-spin ferric heme iron center to heme-bound $^{13}C^{15}N$ (*40*). The ^{15}N NMR signal of APX was found at 585 ppm from $^{15}NO_3^-$ (Table 1). Similarly, for CcP, LiP, and MnP, the ^{15}N NMR signals were observed at 605, 626, and 654 ppm from $^{15}NO_3^-$, respectively (Table 1), which were comparable to previously reported numbers (*46, 56*).

Although ^{13}C and ^{15}N NMR shifts of heme-bound $^{13}C^{15}N$ for many heme proteins showed little species variation (*39*−*41*), those for peroxidases varied depending on the origin of peroxidase. It is worth noting the ^{13}C NMR shift increases in the order of class I, class III, and class II. In paramagnetic ^{13}C NMR spectroscopy, the ^{13}C NMR paramagnetic shift of heme-bound $^{13}C^{15}N$ signal increases with a decrease in the electron-donating character of the axial ligand (*39*−*41*). This is because of the trans ligand effect, in which the binding of cyanide coordinated at the opposite position of the proximal His becomes strong as the donor effect of the proximal His is weak. Therefore, with a decrease in the donor effect, the spin density on the ^{13}C atom polarized by the ferric iron center would be larger, leading to larger paramagnetic shift of the ^{13}C NMR signal. The present ^{13}C NMR results indicate that the electron donor effects of the proximal histidines of these peroxidases vary among the classes, origins of peroxidases, and increase in the order of LiP ≈ MnP < ARP < HRP < APX < CcP. On the other hand, the ^{15}N NMR chemical shift of heme-bound $^{13}C^{15}N$ reflects two distinct factors: the strength of the hydrogen bond(s) to the heme-bound cyanide from the distal side and the electron donation character of the proximal ligand. As shown in previous papers, the hydrogen-bonding effect from the distal side can be estimated from the absolute value of the ratio of the ^{15}N and ^{13}C NMR contact shifts ($^{15}N/^{13}C$) (*39*−*41*). When the hydrogen-bonding effect from the distal side is not present, the ratio would be similar for all heme proteins because the donor effect of the proximal ligand changes the ^{13}C and ^{15}N NMR shifts in a similar ratio. However, the ratio becomes smaller as the hydrogen-bonding effect increases, because the distal residue interacts with the N atom of heme-bound $^{13}C^{15}N$ and, thus, the hydrogen-bonding effect decreases the spin density of the ^{15}N atom of heme-bound $^{13}C^{15}N$ more than that of the ^{13}C atom. The ^{13}C and ^{15}N NMR contact shifts of heme-bound cyanide of peroxidases were calculated from the observed NMR shifts as reported previously (*40*). Details are described in Materials and Methods. As summarized in Table 1, the ratios in peroxidases were almost the same, but much lower than those in other protein families, indicating peroxidases possess a very strong hydrogen-bonding interaction with heme-bound $^{13}C^{15}N$, as suggested by their X-ray crystal structures (*53, 57*). The plot of $^{15}N/^{13}C$ values against the ^{13}C NMR chemical shifts of peroxidases and other heme proteins (globins, cytochrome *c*, heme oxygenase, and FixL) clearly revealed the heme environment is unique to each protein family (Figure 3). Overall, this study clearly demonstrated that peroxidases possess both strong push and pull effects when compared to other heme proteins and that the strength of the pull effects among peroxidases is uniformly strong, while the strength of the push effect is different.

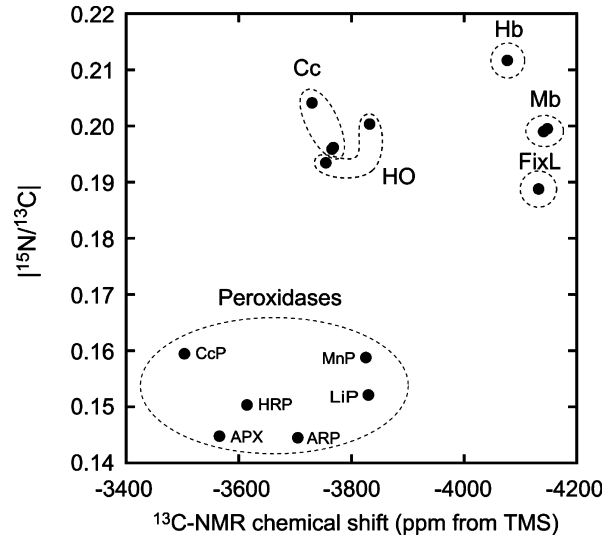

FIGURE 3: Plot of ^{13}C NMR chemical shifts versus $^{15}N/^{13}C$ for heme proteins. Key: Cc, cytochrome *c*; HO, heme oxygenase; Hb, hemoglobin; Mb, myoglobin. Each protein family is circled by a dotted line.

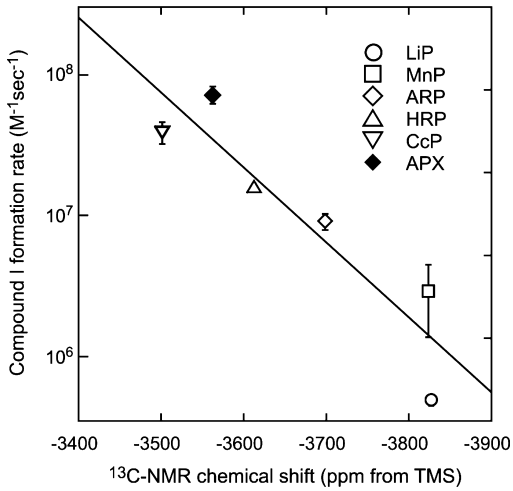

FIGURE 4: Semilogarithmic plot of the compound I formation rates against ^{13}C NMR chemical shifts of various peroxidases. Compound I formation rates for peroxidases were obtained from previous reports: APX (*16*−*19*), CcP (*20*−*23*), ARP (*24*−*26*), LiP (*27*−*30*), MnP (*31*−*34*), and HRP (*35*−*38*). Exceptionally, one of the rates for ARP was determined in this study. An average of four previously reported rates and the deviation are shown for each enzyme.

Correlation between the Push and Pull Effects and the Compound I Formation Rate. To reveal the mechanism of how to control the compound I formation rate, we examined the correlation between the push and pull effects and the compound I formation rate. The average compound I formation rates, calculated using data from at least four studies, were utilized (see Table 1) (*16*−*38*). Because the availability of kinetic data for ARP/CIP at a pH value of 7.0−8.0 is limited, the compound I formation rate for ARP was determined using the transient-state kinetic technique. Using the same sample as was used in the NMR analysis, the rate was measured and calculated to be 1.0×10^7 M^{-1} s^{-1} at pH 7.0. As shown in Figure 4, the semilogarithmic plot of the compound I formation rates against ^{13}C NMR chemical shifts (the push effect) revealed a good correlation with a correlation coefficient of 0.78. As discussed in the above section, since the ^{13}C NMR shift of heme-bound $^{13}C^{15}N$ correlates to the electron donor effect (the push effect) of the proximal His, the correlation means that the compound I formation rate increases with an increase in the push effect of the proximal His. However, as expected from the constant $^{15}N/^{13}C$ value, the semilogarithmic plot of compound I formation rates against the $^{15}N/^{13}C$ value (the pull effect) did not show any correlation (data not shown). These results indicate that a variation in the compound I formation rate of peroxidase results from the difference in the push effect for each peroxidase.

The observed correlation can be explained by molecular orbital diagrams shown in Figure 5. With coordination of hydrogen peroxide (hydroperoxide) to ferric heme iron, the hydroperoxide donates electrons from its occupied p_π* orbital to the unoccupied Fe($3d_z$) orbital (σ-donation) and accepts electrons from the occupied Fe($3d_\pi$) orbital to its unoccupied p_σ* orbital (π-back-donation). Since the σ-donation is more significant than the π-back-donation, the electron density of the heme-bound hydroperoxide becomes smaller with the coordination. However, as an increase in the electron donor effect (σ-donor effect) of the proximal His, the binding of

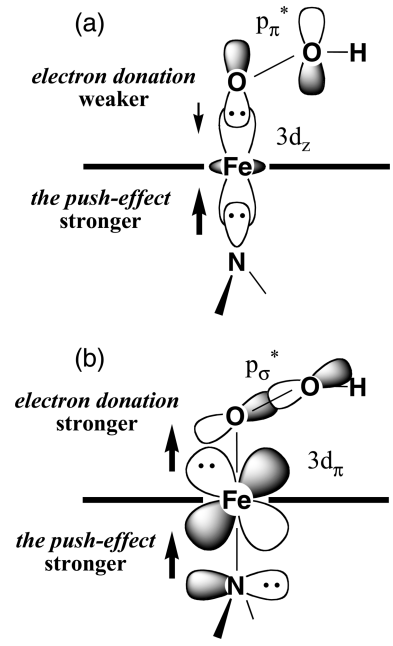

FIGURE 5: Molecular orbital diagram of the ferric heme−hydroperoxide complex for (a) σ-donor effect from the proximal His and (b) π-donor effect from the proximal His. The bold line indicates the heme plane.

hydroperoxide becomes weak, and thus, the σ-donation from the heme-bound hydroperoxide to the heme iron decreases (trans ligand effect). This is the same effect discussed for the ^{13}C NMR shift in the above section. Furthermore, the π-back-donation from the heme iron to the heme-bound hydroperoxide increases with an increase in the π-electron donor effect of the proximal His, because the electron donation from the imidazole π-orbital increases energy of the occupied Fe($3d_\pi$) orbital. These effects increase the electron density (negative charge) in the unoccupied p_σ* and p_π* orbitals of the heme-bound hydroperoxide, leading to polarization and unstableness of the O−O bond. As a result, the heterolytic O−O bond cleavage to form compound I becomes faster as the push effect of the proximal His is stronger.

As far as we know, our data are the first quantitative demonstration of the relationships between the push effect and compound I formation rates among peroxidases. This result is consistent with those obtained using the model compound; the rate of the heterolytic cleavage of peracid was enhanced by electron-rich axial ligands (*58*). In contrast, it was reported that a major determinant of the heterolysis/homolysis of the O−O bond in peroxide is solvent polarity: heterolysis predominates in CH_2Cl_2 and homolysis in toluene (*59*−*61*). A polar solvent system functions as the distal polar region of peroxidases. The results of the present study indicate that peroxidases share a strong pull effect (Figure 3). Therefore, the strong pull effect is the essential driving force for heterolytic cleavage of the O−O bond of peroxides. Indeed, both heterolysis and homolysis of hydrogen peroxide were observed in the reaction between the distal His to Leu mutant of HRP and hydrogen peroxide (*62*). Our data also showed that the strong pull effect is conserved among peroxidases and, thus, supports these previous reports. In summary, the push effect of the proximal ligand correlates well with compound I formation rates while the pull effect from the distal side is a common characteristic of peroxidases.

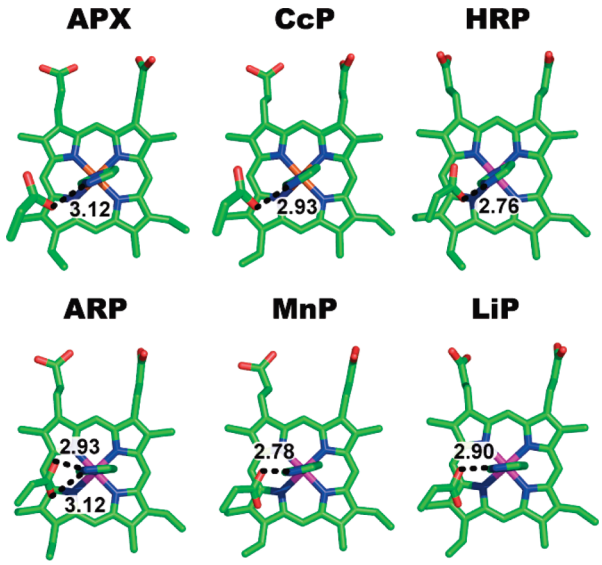

FIGURE 6: Orientation of the proximal imidazole plane and possible hydrogen bond distances between the NH moiety of the proximal imidazole and Asp in various peroxidases. Views of heme from the proximal His and Asp were created from the crystal structures of CcP (PDB code 2CYP) (*2*), APX (1APX) (*3*), HRP (1ATJ) (*4*), ARP (1ARP) (*5*), MnP (1MNP) (*6*), and LiP (1LGA) (*7*) using the Pymol Molecular Graphic System (*63*).

Structural Interpretation of the Push Effect in Peroxidases. The variation in the push effect of peroxidases could be explained by the orientation of the imidazole plane of the proximal His relative to the heme plane and/or by the strength of the hydrogen bond between the proximal His and Asp (*40*). Figure 6 shows differences in the orientation of the imidazole plane relative to the N−Fe−N axis of heme among the peroxidases used in this study. Interestingly, orientation of the proximal imidazole plane is almost conserved in each class of peroxidase. In class I and III peroxidases, the imidazole plane of the proximal His has a parallel orientation to the N−Fe−N axis of heme, while in class II peroxidases, the imidazole plane has a staggered conformation to the N−Fe−N axis. The parallel orientation of the proximal His imidazole plane to the N−Fe−N axis of heme overlaps the π orbital of the imidazole nitrogen atom and the heme iron d_π orbital, which strengthens the electronic interaction between the proximal His and the heme iron. On the other hand, the staggered conformation cannot overlap the π orbital of the imidazole nitrogen atom and the heme iron d_π orbital, which weakens the electronic interaction between the proximal His and the heme iron. As a result, in class I and III peroxidases (APX, CcP, and HRP), the electron push effect from the proximal His is much more effectively conveyed to the heme iron, but not in class II peroxidases (LiP, MnP and ARP). As discussed in the above section, the lack of the π-donor effect of the proximal His in class II peroxidases is reasonable to the slow compound I formation.

The orientation of the imidazole plane is determined by the mode of the hydrogen-bonding interaction with the proximal Asp. In class I and III peroxidases (CcP, APX, and HRP), the Oδ1 of the carboxylate in the Asp forms a hydrogen-bonding interaction with the NH moiety of the proximal His, locking the imidazole plane in a parallel conformation. In contrast, in class II peroxidase, the Asp Oδ2, rather than the Oδ1, is involved in the hydrogen-bonding interaction, inducing a rotation of the imidazole plane to a staggered conformation. Although overall tertiary structures of peroxidases are well conserved among all classes, small differences in the primary structures among the three classes induce a small shift of the Asp, leading to such small differences in the mode of the hydrogen-bonding interaction and the push effect of the proximal ligand (*2*−*7*). While either Oδ1 or Oδ2 in the proximal Asp interacts with the proximal imidazole in most peroxidases, both Oδ1 and Oδ2 interact with the proximal imidazole in ARP (Figure 6). This interaction may explain a stronger push effect in ARP than in the other class II peroxidases, LiP and MnP (Table 1).

CONCLUSION

A comparative analysis of the members of the plant peroxidase superfamily using paramagnetic ^{13}C and ^{15}N NMR spectroscopy revealed that the electron donation characteristics (the push effect) of each peroxidase differ significantly while these peroxidases have uniformly strong hydrogen bonding to the bound hydroperoxide (the pull effect). The relationship observed between compound I formation rates and the push effect can be explained by orientation of the proximal imidazole plane.

REFERENCES

1. Dunford, H. B. (1999) *Heme Peroxidases*, John Wiley and Sons, New York, NY.
2. Finzel, B. C., Poulos, T. L., and Kraut, J. (1984) Crystal Structure of Yeast Cytochrome *c* Peroxidase Refined at 1.7-Å Resolution. *J. Biol. Chem. 259*, 13027–13036.
3. Patterson, W. R., and Poulos, T. L. (1995) Crystal Structure of Recombinant Pea Cytosolic Ascorbate Peroxidase. *Biochemistry 34*, 4331–4341.
4. Gajhede, M., Schuller, D. J., Henriksen, A., Smith, A. T., and Poulos, T. L. (1997) Crystal Structure of Horseradish Peroxidase C at 2.15 Å Resolution. *Nat. Struct. Biol. 4*, 1032–1038.
5. Kunishima, N., Fukuyama, K., Matsubara, H., Hatanaka, H., Shibano, Y., and Amachi, T. (1994) Crystal Structure of the Fungal Peroxidase from *Arthromyces ramosus* at 1.9 Å Resolution. Structural Comparisons with the Lignin and Cytochrome *c* Peroxidases. *J. Mol. Biol. 235*, 331–344.
6. Sundaramoorthy, M., Kishi, K., Gold, M. H., and Poulos, T. L. (1994) The Crystal Structure of Manganese Peroxidase from *Phanerochaete chrysosporium* at 2.06-Å Resolution. *J. Biol. Chem. 269*, 32759–32767.
7. Poulos, T. L., Edwards, S. L., Wariishi, H., and Gold, M. H. (1993) Crystallographic Refinement of Lignin Peroxidase at 2 Å. *J. Biol. Chem. 268*, 4429–4440.
8. Poulos, T. L., and Kraut, J. (1980) The Stereochemistry of Peroxidase Catalysis. *J. Biol. Chem. 255*, 8199–8205.
9. Hiner, A. N., Raven, E. L., Thorneley, R. N., García-Cánovas, F., and Rodríguez-López, J. N. (2002) Mechanisms of Compound I Formation in Heme Peroxidases. *J. Inorg. Biochem. 91*, 27–34.
10. Poulos, T. L. (1987) Heme enzyme crystal structures. *Adv. Inorg. Biochem. 7*, 1–36.
11. Dawson, J. H. (1988) Probing structure-function relations in heme-containing oxygenases and peroxidases. *Science 240*, 433–439.
12. Goodin, D. B., and McRee, D. E. (1993) The Asp-His-Fe triad of cytochrome *c* peoxidase controls the reduction potential, electronic structure, and coupling of the tryptophan free radical to the heme. *Biochemistry 40*, 1274–1283.
13. Hirst, J., Wilcox, S. K., Ai, J., Monne-Loccoz, P., Loehr, T. M., and Goodin, D. B. (2001) Replacement of the Axial Histidine Ligand with Imidazole in Cytochrome *c* Peroxidase. 2. Effects on Heme Coordination and Function. *Biochemistry 40*, 1274–1283.
14. Erman, J. E., Vitello, L. B., Miller, M. A., Shaw, A., Brown, K. A., and Kraut, J. (1993) Histidine 52 Is a Critical Residue for Rapid Formation of Cytochrome *c* Peroxidase Compound I. *Biochemistry 32*, 9798–9806.
15. de Ropp, J. S., Sham, S., Asokan, A., Newmyer, S., Ortiz de Montellano, P. R., and La Mar, G. N. (2002) Influence of the Distal

His in Imparting Imidazolate Character to the Proximal His in Heme Peroxidase: ^{1}H NMR Spectroscopic Study of Cyanide-Inhibited His42→Ala Horseradish Peroxidase. *J. Am. Chem. Soc. 124*, 11029–11037.

16. Mandelman, D., Jamal, J., and Poulos, T. L. (1998) Identification of Two Electron-Transfer Sites in Ascorbate Peroxidase Using Chemical Modification, Enzyme Kinetics, and Crystallography. *Biochemistry 37*, 17610–17617.
17. Macdonald, I. K., Badyal, S. K., Ghamsari, L., Moody, P. C., and Raven, E. L. (2006) Interaction of Ascorbate Peroxidase with Substrates: A Mechanistic and Structural Analysis. *Biochemistry 45*, 7808–7817.
18. Marquez, L. A., Quitoriano, M., Zilinskas, B. A., and Dunford, H. B. (1996) Kinetic and Spectral Properties of Pea Cytosolic Ascorbate Peroxidase. *FEBS Lett. 389*, 153–156.
19. Lad, L., Mewies, M., Basran, J., Scrutton, N. S., and Raven, E. L. (2002) Role of Histidine 42 in Ascorbate Peroxidase. Kinetic Analysis of the H42A and H42E Variants. *Eur. J. Biochem. 269*, 3182–3192.
20. Loo, S., and Erman, J. E. (1975) A Kinetic Study of the Reaction between Cytochrome *c* Peroxidase and Hydrogen Peroxide. Dependence on pH and Ionic Strength. *Biochemistry 14*, 3467–3470.
21. Erman, J. E., Vitello, L. B., Miller, M. A., and Kraut, J. (1992) Active-Site Mutations in Cytochrome *c* Peroxidase: A Critical Role for Histidine-52 in the Rate of Formation of Compound I. *J. Am. Chem. Soc. 114*, 6592–6593.
22. Goodin, D. B., Davidson, M. G., Roe, J. A., Mauk, A. G., and Smith, M. (1991) Amino Acid Substitutions at Tryptophan-51 of Cytochrome *c* Peroxidase: Effects on Coordination, Species Preference for Cytochrome *c*, and Electron Transfer. *Biochemistry 30*, 4953–4962.
23. Choudhury, K., Sundaramoorthy, M., Hickman, A., Yonetani, T., Woehl, E., Dunn, M. F., and Poulos, T. L. (1994) Role of the Proximal Ligand in Peroxidase Catalysis. Crystallographic, Kinetic, and Spectral Studies of Cytochrome *c* Peroxidase Proximal Ligand Mutants. *J. Biol. Chem. 269*, 20239–20249.
24. Abelskov, A. K., Smith, A. T., Rasmussen, C. B., Dunford, H. B., and Welinder, K. G. (1997) pH Dependence and Structural Interpretation of the Reactions of *Coprinus cinereus* Peroxidase with Hydrogen Peroxide, Ferulic Acid, and 2,2′-Azinobis(3-ethylbenzothiazoline-6-sulfonic acid). *Biochemistry 36*, 9453–9463.
25. Di Cerbo, P., Welinder, K. G., and Schiødt, C. B. (2001) Kinetic Evidence for Surface Residues Influencing the Active Site of *Coprinus cinereus* Peroxidase: Analysis of the pH Dependence of G154E, P90H and P90H-G154E Substrate Entrance Mutants. *Biochim. Biophys. Acta 1544*, 18–27.
26. Andersen, M. B., Hsuanyu, Y., Welinder, K. G., Schneider, P., and Dunford, H. B. (1991) Spectral and Kinetic-Properties of Oxidized Intermediates of *Coprinus cinereus* Peroxidase. *Acta Chem. Scand. 45*, 1080–1086.
27. Johjima, T., Wariishi, H., and Tanaka, H. (2002) Veratryl Alcohol Binding Sites of Lignin Peroxidase from *Phanerochaete chrysosporium*. *J. Mol. Catal. B: Enzymat. 17*, 49–57.
28. Andrawis, A., Johnson, K. A., and Tien, M. (1988) Studies on Compound I Formation of the Lignin Peroxidase from *Phanerochaete chrysosporium*. *J. Biol. Chem. 263*, 1195–1198.
29. Doyle, W. A., Blodig, W., Veitch, N. C., Piontek, K., and Smith, A. T. (1998) Two Substrate Interaction Sites in Lignin Peroxidase Revealed by Site-Directed Mutagenesis. *Biochemistry 37*, 15097–15105.
30. Sollewijn Gelpke, M. D., Mayfield-Gambill, M., Lin Cereghino, G. P., and Gold, M. H. (1999) Homologous Expression of Recombinant Lignin Peroxidase in *Phanerochaete chrysosporium*. *Appl. Environ. Microbiol. 65*, 1670–1674.
31. Wariishi, H., Dunford, H. B., MacDonald, I., and Gold, M. H. (1989) Manganese Peroxidase from the Lignin-Degrading Basidiomycete *Phanerochaete chrysosporium*. Transient State Kinetics and Reaction Mechanism. *J. Biol. Chem. 264*, 3335–3340.
32. Kishi, K., Kusters-van Someren, M., Mayfield, M. B., Sun, J., Loehr, T. M., and Gold, M. H. (1996) Characterization of Manganese (II) Binding Site Mutants of Manganese Peroxidase. *Biochemistry 35*, 8986–8994.
33. Whitwam, R. E., Koduri, R. S., Natan, M., and Tien, M. (1999) Role of Axial Ligands in the Reactivity of Mn Peroxidase from *Phanerochaete chrysosporium*. *Biochemistry 38*, 9608–9616.
34. Ambert-Balay, K., Dougherty, M., and Tien, M. (2000) Reactivity of Manganese Peroxidase: Site-Directed Mutagenesis of Residues in Proximity to the Porphyrin Ring. *Arch. Biochem. Biophys. 382*, 89–94.
35. Rodríguez-López, J. N., Smith, A. T., and Thorneley, R. N. (1996) Role of Arginine 38 in Horseradish Peroxidase. A Critical Residue for Substrate Binding and Catalysis. *J. Biol. Chem. 271*, 4023–4030.
36. Nagano, S., Tanaka, M., Ishimori, K., Watanabe, Y., and Morishima, I. (1996) Catalytic Roles of the Distal Site Asparagine-Histidine Couple in Peroxidases. *Biochemistry 35*, 14251–14258.
37. Araiso, T., and Dunford, H. B. (1980) Horseradish Peroxidase. XLI. Complex Formation with Nitrate and Its Effect upon Compound I Formation. *Biochem. Biophys. Res. Commun. 94*, 1177–1182.
38. Dunford, H. B., Hweson, W. D., and Steiner, H. (1978) Horseradish-Peroxidase 29. Reactions in Water and Deuterium-oxide−Cyanide Binding, Compound-I Formation, and Reactions of Compound-I and Compound-II with Ferrocyanide. *Can. J. Chem. 56*, 2844–2852.
39. Fujii, H. (2002) ^{13}C NMR Signal Detection of Iron-Bound Cyanide Ions in Ferric Cyanide Complexes of Heme Proteins. *J. Am. Chem. Soc. 124*, 5936–5937.
40. Fujii, H., and Yoshida, T. (2006) ^{13}C and ^{15}N NMR Studies of Iron-Bound Cyanides of Heme Proteins and Related Model Complexes: Sensitive Probe for Detecting Hydrogen-Bonding Interactions at the Proximal and Distal Sides. *Inorg. Chem. 45*, 6816–6827.
41. Tanaka, A., Nakamura, H., Shiro, Y., and Fujii, H. (2006) Roles of the Heme Distal Residues of FixL in O_2 Sensing: A Single Convergent Structure of the Heme Moiety Is Relevant to the Downregulation of Kinase Activity. *Biochemistry 45*, 2515–2523.
42. Glenn, J. K., and Gold, M. H. (1985) Purification and Characterization of an Extracellular Mn(II)-Dependent Peroxidase from the Lignin-Degrading Basidiomycete *Phanerochaete chrysosporium*. *Arch. Biochem. Biophys. 242*, 329–341.
43. Wariishi, H., and Gold, M. H. (1990) Lignin Peroxidase Compound III. Mechanism of Formation and Decomposition. *J. Biol. Chem. 265*, 2070–2077.
44. Wariishi, H., Marquez, L., Dunford, H. B., and Gold, M. H. (1990) Lignin Peroxidase Compounds II and III. Spectral and Kinetic Characterization of Reactions with Peroxides. *J. Biol. Chem. 265*, 11137–11142.
45. Bonnarme, P., and Jeffries, T. W. (1990) Mn(II) Regulation of Lignin Peroxidases and Manganese-Dependent Peroxidases from Lignin-Degrading White Rot Fungi. *Appl. Environ. Microbiol. 56*, 210–217.
46. Banci, L., Bertini, I., Kuan, I. C., Tien, M., Turano, P., and Vila, A. J. (1993) NMR Investigation of Isotopically Labeled Cyanide Derivatives of Lignin Peroxidase and Manganese Peroxidase. *Biochemistry 32*, 13483–13489.
47. Teske, J. G., Savenkova, M. I., Mauro, J. M., Erman, J. E., and Satterlee, J. D. (2000) Yeast Cytochrome *c* Peroxidase Expression in *Escherichia coli* and Rapid Isolation of various Highly Pure Holoenzymes. *Protein Expression Purif. 19*, 139–147.
48. Dalton, D. A., Diaz del Castillo, L., Kahn, M. L., Joyner, S. L., and Chatfield, J. M. (1996) Heterologous Expression and Characterization of Soybean Cytosolic Ascorbate Peroxidase. *Arch. Biochem. Biophys. 328*, 1–8.
49. Goff, H. M. (1977) Carbon-13 Nuclear Magnetic Resonance Spectroscopy of Iron(III) Porphyrin-Cyanide Complexes. Location of the Bound Cyanide Ion Resonance. *J. Am. Chem. Soc. 99*, 7723–7725.
50. Herbinson-Evans, D., and Richrads, R. E. (1964) ^{14}N Chemical Shifts in Organic Compounds. *Mol. Phys. 8*, 19–31.
51. Morita, Y., and Mason, H. S. (1965) An Electron Spin Resonance Study of Some Hemoproteins. *J. Biol. Chem. 240*, 2654–2659.
52. Henriksen, A., Smith, A. T., and Gajhede, M. (1999) The Structures of the Horseradish Peroxidase C-Ferulic Acid Complex and the Ternary Complex with Cyanide Suggest How Peroxidases Oxidize Small Phenolic Substrates. *J. Biol. Chem. 274*, 35005–35011.
53. Fukuyama, K., Kunishima, N., Amada, F., Kubota, T., and Matsubara, H. (1995) Crystal Structures of Cyanide- and Triiodide-Bound Forms of *Arthromyces ramosus* Peroxidase at Different pH Values. Perturbations of Active Site Residues and their Implication in Enzyme Catalysis. *J. Biol. Chem. 270*, 21884–21892.
54. Banci, L., Bertini, I., Pease, E. A., Tien, M., and Turano, P. (1992) ^{1}H NMR Investigation of Manganese Peroxidase from *Phanerochaete chrysosporium*. A Comparison with Other Peroxidases. *Biochemistry 31*, 10009–10017.

55. Satterlee, J. D., Erman, J. E., LaMar, G. N., Smith, K. M., and Langry, K. C. (1983) Assignment of Hyperfine Shifted Resonances in High-Spin Forms of Cytochrome *c* Peroxidase by Reconstitutions with Deuterated Hemins. *Biochim. Biophys. Acta 743*, 246–255.
56. Ferrer, J. C., Turano, P., Banci, L., Bertini, I., Morris, I. K., Smith, K. M., Smith, M., and Mauk, A. G. (1994) Active Site Coordination Chemistry of the Cytochrome *c* Peroxidase Asp235Ala Variant: Spectroscopic and Functional Characterization. *Biochemistry 33*, 7819–7829.
57. Edwards, S. L., and Poulos, T. L. (1990) Ligand Binding and Structural Perturbations in Cytochrome *c* Peroxidase. A Crystallographic Study. *J. Biol. Chem. 265*, 2588–2595.
58. Yamaguchi, K., Watanabe, Y., and Morishima, I. (1993) Direct Observation of the Push Effect on the Oxygen-Oxygen Bond Cleavage of Acylperoxoiron(III) Porphyrin Complexes. *J. Am. Chem. Soc. 115*, 4058–4065.
59. Groves, J. T., and Watanabe, Y. (1986) Oxygen Activation by Metalloporphyrins Related to Peroxidase and Cytochrome P-450. Direct Observation of the Oxygen-Oxygen Bond Cleavage Step. *J. Am. Chem. Soc. 108*, 7834–7836.
60. Groves, J. T., and Watanabe, Y. (1988) Reactive Iron Porphyrin Derivatives Related to the Catalytic Cycles of Cytochrome P-450 and Peroxidase. Studies of the Mechanism of Oxygen Activation. *J. Am. Chem. Soc. 110*, 8443–8452.
61. Watanabe, Y., Yamaguchi, K., Morishima, I., Takehira, K., Shimizu, M., Hayakawa, T., and Orita, H. (1991) Remarkable Solvent Effect on the Shape-Selective Oxidation of Olefins Catalyzed by Iron(III) Porphyrins. *Inorg. Chem. 30*, 2581–2582.
62. Rodríguez-López, J. N., Lowe, D. J., Hernández-Ruiz, J., Hiner, A. N., García-Cánovas, F., and Thorneley, R. N. (2001) Mechanism of Reaction of Hydrogen Peroxide with Horseradish Peroxidase: Identification of Intermediates in the Catalytic Cycle. *J. Am. Chem. Soc. 123*, 11838–11847.
63. DeLano, W. L. (2008) The Pymol Molecular Graphic System, DeLano Scientific LLC, Palo Alto, CA.

BI802030A